The Astrophysical Journal, 850:117 (13pp), 2017 December 1 https://doi.org/10.3847/1538-4357/aa947d

A Study of GRBs with Low-luminosity Afterglows

H. Dereli[1,2], M. Boër[2], B. Gendre[2,3,4], L. Amati[5], S. Dichiara[6], and N. B. Orange[4,7]
[1] Department of Physics, Royal Institute of Technology (KTH), AlbaNova, SE-106 91 Stockholm, Sweden; husne@kth.se
[2] ARTEMIS (CNRS UMR 7250, OCA, UNS); Boulevard de l'Observatoire, CS 34229, F-06304 Nice Cedex 4, France
[3] University of Virgin Islands, 2 John Brewer's Bay Road, St. Thomas 00802, USVI, USA
[4] Etelman Observatory, Bonne Resolution, St. Thomas 00802, USVI, USA
[5] IASF-Bologna/INAF; Area della Ricerca di Bologna, Via Gobetti 101, I-40129, Bologna, Italy
[6] University of Ferrara; Via Savonarola 9, I-44121 Ferrara, Italy
[7] OrangeWave Innovative Science, LLC, Moncks Corner, SC 29461, USA
Received 2016 November 9; revised 2017 October 4; accepted 2017 October 14; published 2017 November 22

Abstract

We present a sample composed of the 41 faintest X-ray afterglows of the population of long gamma-ray bursts (lGRBs) with known redshift. We study their intrinsic properties (spectral index, decay index, distance, luminosity, isotropic radiated energy, and peak energy) and their luminosity distribution functions to assess whether they belong to the same population as the brighter afterglow events. We find that these events belong to a population of nearby ones, different from the general population of lGRBs. In addition, these events are faint during their prompt phase, and include the few possible outliers of the Amati relation.

Key words: gamma-ray burst: general – methods: data analysis – X-rays: general

1. Introduction

Gamma-ray bursts (GRBs) are the most luminous events in the universe, with observed isotropic luminosities ranging from 10^{49} to 10^{52} erg s^{-1} (for reviews, see Mészáros 2006; Kumar & Zhang 2015; Pe'er 2015). GRBs display two phases sequentially: first, the prompt emission followed by the afterglow phase (Rees & Mészáros 1992; Mészáros & Rees 1997; Panaitescu et al. 1998), each of which is observable at many wavelengths (e.g., Costa et al. 1997; Frail et al. 1997; Van Paradijs et al. 1997). In X-rays, their light curve can be described as a steep-flat-steep broken power law (Nousek et al. 2006), whose first part (the steep decay) has been associated with the prompt phase (Barthelmy et al. 2005; Tagliaferri et al. 2005; Zhang et al. 2006; Willingale et al. 2007), through high latitude emission. Observations obtained prior to the steep decay, such as from rapid followups or long-duration bursts, provide insight to the line-of-sight prompt emission. The portion of their light curves following the steep decay is thought to be due to the dynamics of the interaction of the jet with the surrounding medium (Panaitescu & Kumar 2000).

It has been realized that at least two distinct populations of GRBs exist. A discovery based on their durations (T_{90}, the duration during which 90% of the prompt phase energy is emitted, Mazets et al. 1981; Dezalay et al. 1992; Kouveliotou et al. 1993), where long bursts (hereafter lGRBs) are associated with a duration larger than 2 s, and short ones (hereafter sGRB) are associated with a duration as short as few milliseconds. Theoretically, it is proposed that long and short GRBs have a different progenitor: the collapse of a very massive star for lGRBs (Woosley 1993) and a compact binary merger for sGRBs (Eichler et al. 1989).

Based on the proposed massive star–lGRB link and the discovery of their afterglow counterpart, studies to standardize the latter phenomena rapidly followed. The first attempt was by Boër & Gendre (2000), in X-rays, which was followed by numerous optical studies (Kann et al. 2006; Liang & Zhang 2006; Nardini et al. 2006) and several attempts seeking a standardization of the prompt phase (e.g., Amati et al. 2002; Ghisellini et al. 2009; Ghisellini 2012). These studies led Gendre & Boër (2005) to define three classes of lGRBs using their afterglow properties; namely, from bright to dim events: groups I, II, and III. Groups I and II were studied in detail by Gendre et al. (2008), while at that time group III was overlooked due to the small number of events.

We have taken advantage of an increased number of lGRBs, observed by *Swift* before the end of 2016 to complete a study of group III events and report their results in this paper.

The paper is organized as follows. In Section 2, we define our sample of low-luminosity afterglow events. In Section 3, we present all the properties of this sample, including their redshift distribution. In Section 4, we then discuss the possible biases and selection effects due to the intrinsic GRB luminosity function distribution, altogether with the possible origin of group III lGRBs. Our conclusions are presented in Section 5. Throughout the remainder of this paper, errors are quoted at the 90% confidence level, and we use a standard flat ΛCDM model with $\Omega_m = 0.3$ and $H_0 = 72$ km s^{-1} Mpc^{-1}, as well as the notation that $F \propto t^{-\alpha}\nu^{-\beta}$.

2. Definition of the Sample of Low-luminosity Afterglow Events

We extended the group III sample defined in Gendre et al. (2008) thanks to *Swift* observations (Gehrels et al. 2004). To avoid biases in our results from changes in the detecting instrument, only those sources detected by *Swift* were used in this study. From among the *Swift* database, we then selected all bursts observed before 2017 January 1, with measured redshifts, whose values were compiled from the list of J. Greiner.[8] This led to a first sample of 371 sources observed at X-ray wavelengths, including short and long GRBs. As we are only interested in the latter, sGRBs were excluded, leaving 326 lGRBs in the global sample. Our data analysis techniques are explained in the Appendix.

[8] http://www.mpe.mpg.de/~jcg/grbgen.html

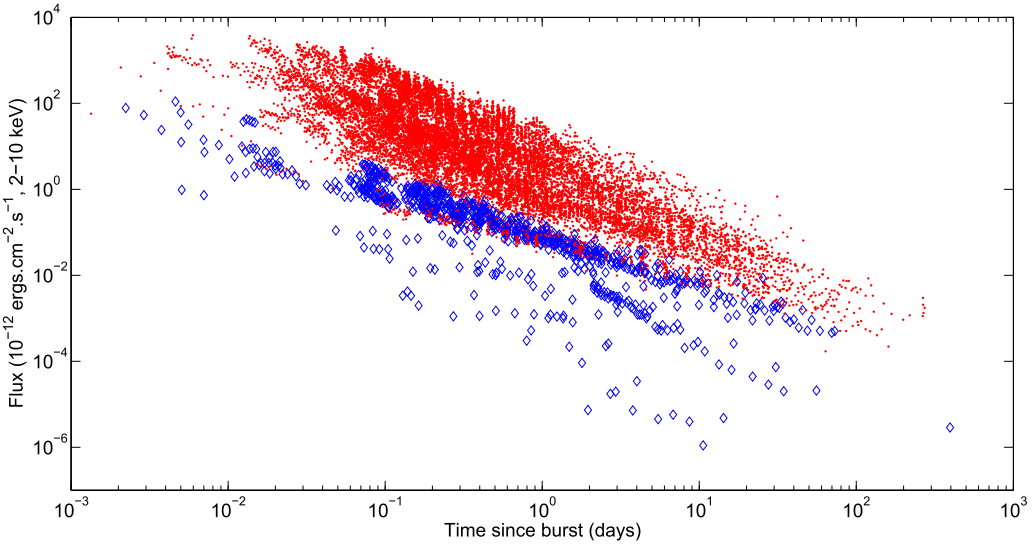

Figure 1. Light curves of all sources, corrected for distance effects (see the text) and rescaled at a common redshift $z = 1$. The group III events are shown with blue diamonds and the control sample is shown with red dots.

Initially, the definition of a group III event was a burst with an X-ray flux lower than 1×10^{-13} erg cm^{-2} s^{-1} (2.0–10.0 keV) one day after the burst (Gendre et al. 2008). To take into account events with no data one day post-event, we extended that definition with two template afterglows. For these templates, we assumed decay indices of 1.2 and 1.4, which correspond to those expected in the case of a wind medium and a constant-density circumburst medium (also referred to as ISM), when $p \sim 2.3$ (p being the power-law index of the distribution of the energy of the accelerated electrons), respectively. All bursts characterized by afterglow light curves entirely below these two templates were considered as members of our group III sample, and the remaining ones were used as a control. These results are displayed in Figure 1.

The final sample includes 41 events, listed in Table 1, representing about 12.5% of all lGRBs considered here. Table 1 displays the GRB name; redshift; galactic and host $N_{\rm H}$; galactic and host A_V; the afterglow temporal and spectral indices; the isotropic and peak energies; and the T_{90} duration. For those afterglows displaying a break after the plateau phase (GRB 060614 and GRB 120729A), the decay index is indicated pre-break.

We note that GRB 060505 and GRB 060614 have been proposed by some authors to be sGRBs (e.g., Kann et al. 2011, and references therein). As such a classification of these bursts has yet to reach a unanimous consensus and they passed our criteria, they were included in our sample (though see Section 4). However, for completeness, statistical calculations were completed with and without these two events, and we report that the outcomes between these approaches were negligible. As such, all results reported below include these two events.

3. Statistical Properties

3.1. The Redshift Distribution

The redshift distribution of our sample is shown in Figure 2, together with the distribution of the control lGRBs. An examination of Figure 2 shows that the group III events appear more nearby than normal lGRBs (the redshift distribution of these last ones peaks around $z = 2.2$, e.g., Jakobsson et al. 2006; Coward et al. 2013). The common statistical parameters (i.e., mean, median, and standard deviation) of these two distributions are presented in Table 2. We also tested the probability that these two distributions are based on the same population via a Kolomogorov–Smirnov test, whose result ($p = 1.69 \times 10^{-15}$) rejects such a hypothesis.

To account for the fact that selection effects plague group III GRBs (see Section 4), as their faintness compared to normal lGRBs implies a detection biases at large distances, we used the faintest group III GRB afterglows in our sample as a means to estimate that their detection could occur up to a distance of $z = 1$. We stress that this is only an afterglow detection threshold for our sample, and no link is assumed between this limit and the ability to detect their prompt emission. We estimated this limit by increasing the redshift of our faintest event to the limit where its resulting flux was comparable to the usual sensitivity limit observed in the XRT instrument. Because normal lGRBs are very bright, they can easily be detected when located at $z < 1$. Consequently, we consider that when restricted to events with $z < 1$, both samples can be considered as complete, thus removing the detection bias. We have recomputed the cumulative redshift distributions for this subsample (see Figure 3), and performed again a Kolmogorov-Smirnov test. It is very unlikely that the two distributions are drawn from the same population ($p = 8.1 \times 10^{-3}$).

3.2. Prompt Phase

We investigated the prompt properties of our sample. For this analysis, whenever possible we used *Fermi* GBM, *Konus-Wind* or *BeppoSAX* data, either from previously published results or by performing our analysis. It is noted that we avoided BAT data in this work, given that its bandwidth is not large enough to derive spectral parameters with a reasonable degree of accuracy. About half of our events had a firm measurement of the prompt parameters. For the remaining events, only upper or lower limits were obtained. We measured the intrinsic peak energy values ($E_{p,i}$) by correcting our E_p results for cosmological effects. These values cluster broadly within the 40–200 keV range.

Table 1
Burst Sample and its Main Characteristics (See the Text)

GRB	z	N_H (10^{21}cm^{-2})		A_V (mag)		Afterglow		log T_a (s)	E_{iso} (10^{52}erg)	$E_{p,i}$ (keV)	T_{90} (s)	References
		Gal	Host	Gal	Host	Temporal index	Spectral index					
GRB 980425	0.0085	0.428	⋯	0.158	0.13 ± 0.09	0.10 ± 0.06	(0.8)	⋯	$(1.3 \pm 0.2) \times 10^{-4}$	55 ± 21	18	(1), (20)
GRB 011121	0.36	0.951	⋯	1.301	0.39 ± 0.14	1.3 ± 0.03	(0.8)	⋯	7.97 ± 2.2	1060 ± 275	28	(2), (21), (22)
GRB 031203	0.105	6.21	⋯	2.82	1.3	0.5 ± 0.1	0.8 ± 0.1	⋯	$(8.2 \pm 3.5) \times 10^{-3}$	158 ± 51	40	(3), (21)
GRB 050126	1.29	0.551	(0.0)	0.142	⋯	$1.1^{+0.6}_{-0.5}$	0.7 ± 0.7	⋯	[0.4-3.5]	>201	24.8	(23)
GRB 050223	0.5915	0.729	(0.0)	0.238	$1.5^{+1.4}_{-1.3}$	0.91 ± 0.03	1.4 ± 0.7	⋯	$(8.8 \pm 4.4) \times 10^{-3}$	110 ± 55	22.5	(4), (24)
GRB 050525A	0.606	0.907	$0.38^{+9.1}_{-0.38}$	0.252	0.36 ± 0.05	1.4 ± 0.1	1.1 ± 0.4	3.8	2.3 ± 0.5	129 ± 12.9	8.8	(5), (25)
GRB 050801	1.38	0.698	(0.0)	0.255	0.3 ± 0.18	1.25 ± 0.13	$1.84^{+0.56}_{-0.53}$	3.2	[0.27-0.74]	<145	19.4	(5), (23)
GRB 050826	0.297	2.17	8^{+6}_{-4}	1.636	⋯	1.13 ± 0.04	1.1 ± 0.4	4.04	[0.023-0.249]	>37	35.5	(23)
GRB 051006	1.059	0.925	(0.0)	0.176	⋯	1.69 ± 0.13	$1.5^{+0.44}_{-0.46}$	2.77	[0.9-4.3]	>193	34.8	(23)
GRB 051109B	0.08	1.3	<2	0.441	⋯	1.1 ± 0.3	0.7 ± 0.4	3.14	⋯	⋯	14.3	
GRB 051117B	0.481	0.46	(0.0)	0.15	<1.4	1.03 ± 0.5	(0.8)	⋯	[0.034-0.044]	<136	9.0	(6), (23)
GRB 060218	0.0331	1.14	6 ± 2	0.388	0.13	$1.3^{+1.1}_{-0.6}$	0.51 ± 0.05	5.0	$(5.4 \pm 0.54) \times 10^{-3}$	4.9 ± 0.49	∼2100	(7), (26)
GRB 060505	0.089	0.175	(0.0)	0.054	∼0.0	1.91 ± 0.2	(0.8)	⋯	$(3.9 \pm 0.9) \times 10^{-3}$	120 ± 12	∼4	(8), (27)
GRB 060614	0.125	0.313	0.5 ± 0.4	0.058	0.11 ± 0.03	$2.0^{+0.3}_{-0.2}$	0.8 ± 0.2	4.64	0.22 ± 0.09	55 ± 45	108.7	(9), (27)
GRB 060912A	0.937	0.420	(0.0)	0.14	0.5 ± 0.3	1.01 ± 0.06	0.6 ± 0.2	3.3	[0.80-1.42]	>211	5.0	(10), (23)
GRB 061021	0.3463	0.452	0.6 ± 0.2	0.152	<0.10	0.97 ± 0.05	1.02 ± 0.06	3.63	⋯	⋯	46.2	(9)
GRB 061110A	0.758	0.494	(0.0)	0.244	<0.10	1.1 ± 0.2	0.4 ± 0.7	3.68	[0.35-0.97]	>145	40.7	(9), (23)
GRB 070419A	0.97	0.24	<10	0.075	0.37 ± 0.19	0.56 ± 0.0	(0.8)	⋯	[0.20-0.87]	<69	115.6	(11), (23)
GRB 071112C	0.823	0.852	<5	0.317	$0.20^{+0.05}_{-0.04}$	1.43 ± 0.05	$0.8^{+0.5}_{-0.4}$	3.0	⋯	⋯	15	(10), (23)
GRB 081007	0.5295	0.143	$0.97^{+6.9}_{-0.97}$	0.043	0.82 ± 0.09	1.23 ± 0.05	$0.99^{+0.88}_{-0.43}$	4.5	0.18 ± 0.02	61 ± 15	10	(3), (28)
GRB 090417B	0.345	0.14	22 ± 3	0.045	>2.5	1.44 ± 0.07	1.3 ± 0.2	3.54	[0.17-0.35]	>70	>260	(12), (23)
GRB 090814A	0.696	0.461	(0.0)	0.206	<0.2	1.0 ± 0.2	(0.8)	3.5	[0.21-0.58]	<114	80	(13), (23)
GRB 100316D	0.059	0.82	(0.0)	0.31	0.434 ± 0.031-1.209 ± 0.093	1.34 ± 0.07	0.5 ± 0.5	⋯	$(6.9 \pm 1.7) \times 10^{-3}$	20 ± 10	292.8	(14), (15), (29)
GRB 100418A	0.6235	0.584	(0.0)	0.194	0.17	1.42 ± 0.09	0.9 ± 0.3	4.82	[0.06-0.15]	<50	7.0	(16) (23)
GRB 101225A	0.847	0.928	(0.0)	0.262	∼0.0	⋯	(0.8)	4.65	[0.68-1.2]	<98	1088	(17), (23)
GRB 110106B	0.618	0.23	(0.0)	0.066	⋯	1.35 ± 0.06	$1.32^{+0.67}_{-0.32}$	4.04	0.73 ± 0.07	194 ± 56	24.8	(30)
GRB 120422A	0.283	0.372	(0.0)	0.093	0.0	1.3 ± 0.3	0.4 ± 0.4	5.07	[0.016-0.032]	<72	5.35	(18), (31)
GRB 120714B	0.3984	0.187	(0.0)	0.026	⋯	1.89 ± 0.02	(0.8)	⋯	0.08 ± 0.02	69 ± 43	159	(23)
GRB 120722A	0.9586	0.298	350^{+230}_{-170}	55.19	⋯	1.2 ± 0.4	1.2 ± 1.2	⋯	[0.51-1.22]	<88	42.4	(23)
GRB 120729A	0.8	1.4	(0.0)	0.449	⋯	2.8 ± 0.2	0.8 ± 0.3	3.9	[0.80-2.0]	>160	71.5	(23)
GRB 130511A	1.3033	0.208	0.0	0.075	⋯	1.67 ± 0.15	$0.62^{+0.56}_{-0.63}$	3.65	⋯	⋯	5.43	
GRB 130831A	0.4791	0.48	$0.84^{+0.74}_{-0.63}$	0.12	0.0	0.84 ± 0.09	$0.77^{+0.15}_{-0.14}$	3.85	1.16 ± 0.12	81.35 ± 8.14	32.5	(19)
GRB 140318A	1.02	0.243	$4.86^{+7.3}_{-4.04}$	0.064	⋯	1.01 ± 0.11	$1.11^{+0.56}_{-0.45}$	2.68	⋯	⋯	8.43	

Table 1
(Continued)

GRB	z	$N_{\rm H}$		Gal	A_V	Afterglow		log T_a	$E_{\rm iso}$	$E_{\rm p,i}$	T_{90}	References
		Gal	Host		Host	Temporal	Spectral	(s)	(10^{52}erg)	(keV)	(s)	
		(10^{21}cm^{-2})			(mag)	index	index					
GRB 140710A	0.558	0.575	$7.68^{+13.7}_{-6.35}$	0.153	⋯	0.77 ± 0.09	$0.93^{+0.73}_{-0.55}$	3.48	⋯	⋯	3.52	
GRB 150727A	0.313	0.738	0.0	0.236	⋯	0.83 ± 0.11	0.99 ± 0.33	3.48	⋯	⋯	88	
GRB 150821A	0.755	0.06	$1.53^{+5.73}_{-4.28}$	0.046	⋯	1.32 ± 0.09	$1.34^{+0.31}_{-0.27}$	3.57	15.37 ± 3.86	614.25 ± 294.84	172.1	
GRB 151029A	1.423	0.314	$1.21^{+4.08}_{-1.21}$	0.058	⋯	1.26 ± 0.09	$1.16^{+0.47}_{-0.31}$	2.64	0.44 ± 0.08	0.44 ± 0.07	8.95	
GRB 151031A	1.167	0.241	$7.13^{+13.7}_{-6.59}$	0.068	⋯	0.91 ± 0.13	$1.16^{+0.64}_{-0.51}$	3.62	⋯	⋯	5.0	
GRB 160117B	0.870	0.438	$1.35^{+2.41}_{-1,35}$	0.181	⋯	0.84 ± 0.05	$0.92^{+0.31}_{-0.27}$	3.08	⋯	⋯	11.53	
GRB 160425A	0.555	0.621	$6.24^{+7.63}_{-4.21}$	0.156	⋯	0.9 ± 0.02	$0.94^{+0.6}_{-0.47}$	2.97	⋯	⋯	304.58	
GRB 161129A	0.645	1.57	$2.23^{+2.49}_{-1.77}$	0.538	⋯	2.46 ± 0.21	$0.81^{+0.23}_{-0.21}$	3.7	1.3 ± 0.2	324 ± 30	35.53	

Note. The spectral and temporal indices for lGRBs before 2006 August are taken from Gendre et al. 2008. For A_V values, see (1) Krühler et al. 2017; (2) Kann et al. 2006; (3) Kann et al. 2016; (4) Mannucci et al. 2011; (5) Kann et al. 2010; (6) Michalowski et al. 2012; (7) Ferrero et al. 2006; (8) Thöne et al. 2008; (9) Zafar et al. 2011; (10) Schady et al. 2012; (11) Melandri et al. 2009; (12) Holland et al. 2010; (13) Greiner et al. 2010; (14) Bufano et al. 2012; (15) Olivares et al. 2012; (16) Marshall et al. 2011; (17) Thöne et al. 2011; (18) Schulze et al. 2014; (19) Cano et al. 2014. For $E_{\rm iso}$ and $E_{\rm p,i}$ values, see (20) Pian et al. 1999; (21) Ulanov et al. 2005; (22) Amati et al. 2009; (23) in this work; (24) Cabrera et al. 2008; (25) Sakamoto et al. 2011; (26) Campana et al. 2006; (27) Amati et al. 2007; (28) Bissaldi et al. 2008; (29) Starling et al. 2011; (30) Bhat 2011; (31) Melandri et al. 2012.

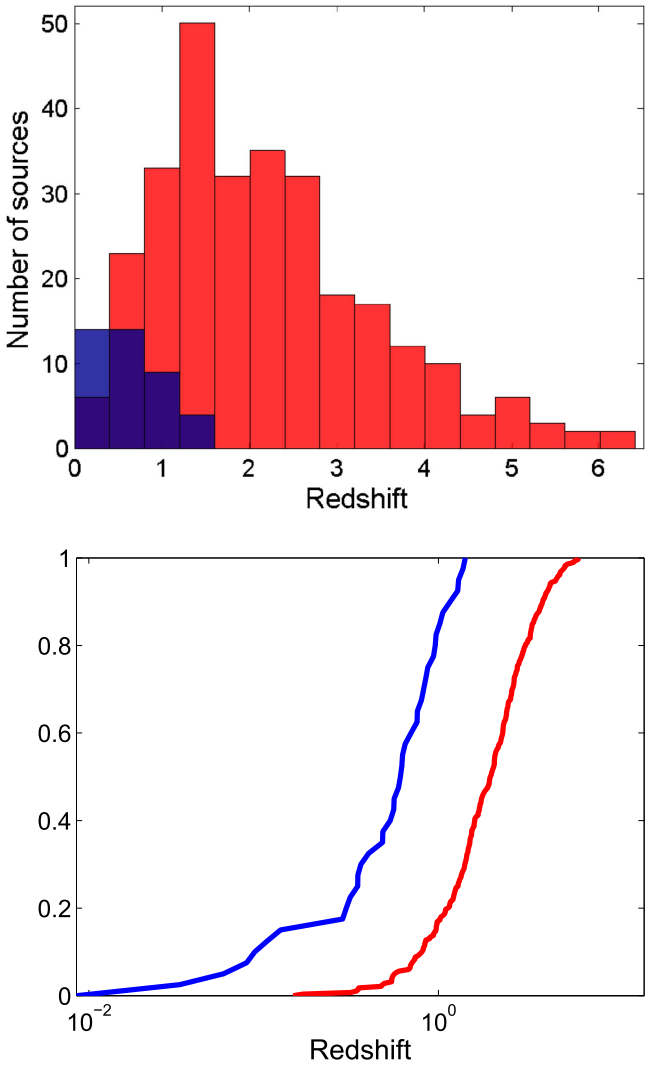

Figure 2. Top: redshift distribution of group III GRBs (blue) compared with normal lGRBs (red). Bottom: cumulative distribution of the same samples.

Table 2
Statistical Parameters of the Redshift Distributions

Parameter	Group III GRBs	All lGRBs
Mean	0.62	2.19
Median	0.66	1.98
Standard deviation	0.39	1.24

We note, however, that there is a lack of bright events in our sample. If one considers the median redshift of group III GRBs, their $E_{p,i}$ values, and intrinsic scatter of the Amati relation, as well as the properties of the BAT instrument, suggest one should expect detecting bursts with a total energy up to $E_{\rm iso} = 3 \times 10^{53}$ erg. Interestingly, such is at least one order of magnitude larger than the brightest measurements listed in Table 1. We conclude that group III GRBs are intrinsically less energetic, both during the prompt and the afterglow phases, compared with normal lGRBs.

3.3. Absorption and Extinction

We checked the distribution of the Milky Way extinction ($A_{V,\rm Gal}$) and absorption ($N_{\rm H,Gal}$) values in the line of sight from our sample of events. Though X-ray absorption has little effect on the selection of our group III sample, as we relied on fluxes in the 2.0–10.0 keV band where absorption can be neglected (Morrison & McCammon 1983), a consistency check of this artifact was performed to confirm its absence in our samples. Here, it is pointed out that in addition, it is well known that the optical extinction can bias a distribution (for instance the well-known problem of dark bursts, e.g., Jakobsson et al. 2004).

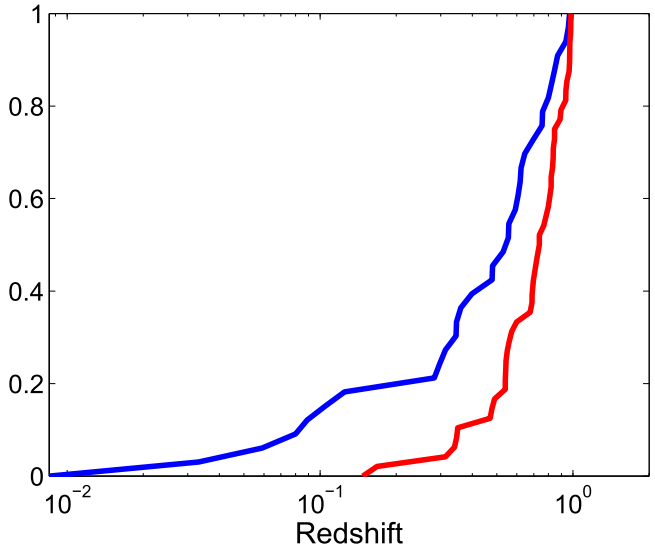

Figure 3. Cumulative distribution of the redshift of the group III GRBs (blue) compared with all lGRBs (red) for redshifts $z < 1$.

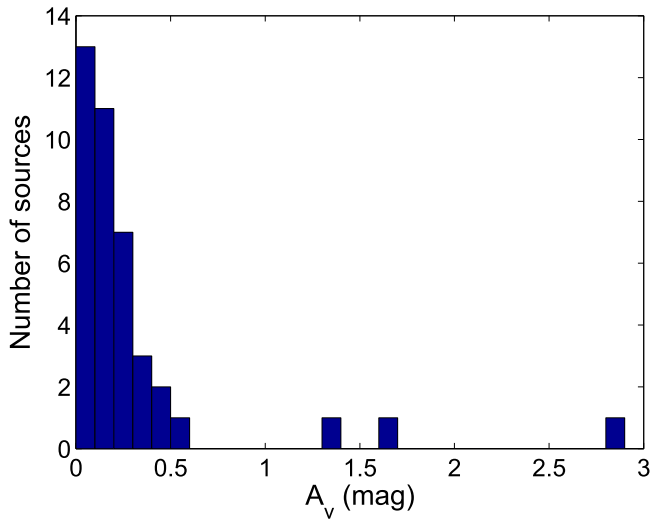

Figure 4. Distribution of the optical extinction A_V in the Galaxy for group III GRBs.

Optical extinctions of our sample were calculated using the *IRSA* tool[9] for the Landolt *V* band measured by Schlafly & Finkbeiner (2011) for all bursts. These computations were done by using the name resolver tool; only in the case of GRB 161129A (not resolved), we used the coordinates of the event (R.A.: 316.19; decl.: +32.12). The results are reported in Figure 4. As can be observed, the distribution is clustered at low extinction values, in line with previous results ($A_V < 2$ for 87% of normal lGRBs, Covino et al. 2013). In fact, because GRBs are extragalactic events, their projected position onto the

[9] http://irsa.ipac.caltech.edu/applications/DUST/

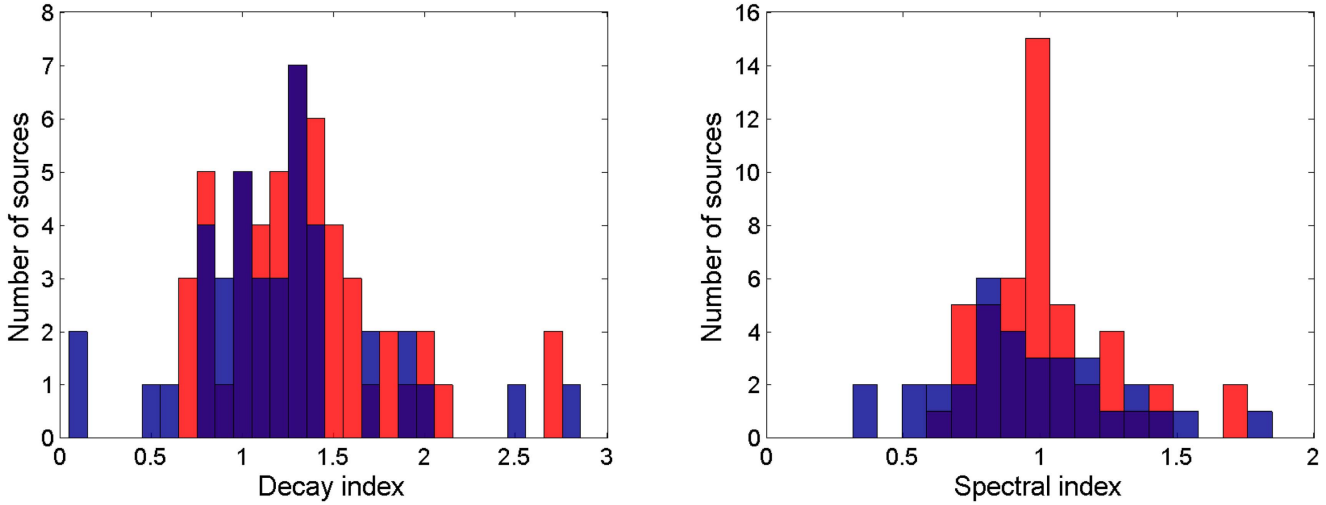

Figure 5. Distribution of the decay index (left) and spectral index (right) for the group III GRBs sample (blue) compared with the reference sample (red).

Galaxy is randomly distributed. As the mean statistics derived from both our samples align with that of the Galaxy, they are considered to have the same properties. We found the same result for our X-ray absorption results. Below, we consider the assumption that the Galaxy's gas and dust did not introduce biases into our group III GRB sample.

We finally investigated the intrinsic hydrogen column density $N_{\rm H}$, as it can be linked to the host properties (Reichart & Price 2002). Most of the values of our group III GRBs were compatible with assumptions of little to no intrinsic absorption. For the sources with a non-zero $N_{\rm H,X}$ (see column 4 in Table 1), the absorption due to the host galaxy was found to be on average a factor of 10 larger than in the Milky Way, as already noted by Starling et al. (2013).

3.4. Decay and Spectral Indices

The distributions of the temporal decay and spectral indices for our sample are presented in Figure 5. The two samples are very similar, as indicated by a K-S test ($p = 0.79$ and $p = 0.29$ for the decay and the spectral indices, respectively). We conclude that the two samples have similar spectral and temporal properties.

4. Discussion

4.1. Selection Effects

It must be recognized that the probability of obtaining successful redshift measures for group III afterglow events is hindered by the fact that faint afterglows can be barely more energetic than the XRT or optical detection thresholds, an assessment that, moreover, is dependent on spectroscopic observations at optical wavelengths. Further contributing to this issue of measuring these burst's redshifts is the temporal decay of their emission, cases of initially dim afterglows, as well as the possibility of host galaxy association even without optical afterglows. The latter association, however, is strongly debated (as there is a significant probability to find a distant galaxy inside a typical XRT or BAT error box) and the prompt/afterglow faintness increases the size of the error box (e.g., GRB 060805A Perley et al. 2009).

On the other hand, we must consider that the volume of the universe at low redshifts is very small, where the few events that do occur appear as strong, nearby beacons. Two famous examples are GRB 030329, whose extraordinarily bright afterglow turned out to be very "normal" in terms of luminosity (Kann et al. 2006) and GRB 130427A, the brightest GRB in 30 years (e.g., Maselli et al. 2014). As any closer normal lGRB could be detected without a problem, we consider it significant that we do see several group III events closer than these normal lGRBs. Moreover, as stated previously, our sample size and duration (more than 10 years) supports the claim that the statistically *observed* population of group III events is closer than those of the normal lGRBs. Thus, we can conclude that we are witnessing two distinct populations in the local universe that can co-exist at larger distances.

Finally, can we consider that our sample is not contaminated by some normal lGRBs? This is a very important aspect, as we are trying to deduce the nature of this population from the observed properties of our sample.

It is pointed out that our selection criteria allowed the discrimination and correct classification of the normal nearby lGRB's GRB 030329 and GRB 130427A from group III events. As such, we find confidence in the fact that the proportion of normal lGRBs remaining in our sample is small enough to allow the main group III event properties to be derived. Last, this implies that our sample is statistically significant due to its size.

4.2. Effect of the Luminosity Distribution Function

The first possible explanation for the difference in the redshift distributions is an effect of the GRB luminosity function. A low-luminosity tail of the luminosity function can introduce a population of sources seen only at low redshift. This is consistent with the choice of D'Avanzo et al. (2012a, see their Figure 2), in which most of the low-luminosity GRBs were removed to have an unbiased sample of "normal" lGRBs. In fact, most studies (e.g., Coward 2005; Howell & Coward 2013; Deng et al. 2016) on the rate of GRBs discarded or separated the low-luminosity events from the sample of high-luminosity GRBs in their computation. To test this hypothesis, we ran a Monte Carlo (MC) simulation using the best-known luminosity and redshift distribution functions from the literature (Liang et al. 2007; Howell & Coward 2013).

We used the redshift distribution from Howell & Coward (2013),

$$\frac{dN}{dz} = \frac{dV(z)}{dz}\,\frac{R_{\rm GRB}(z)}{1+z}\,dz\ , \tag{1}$$

where $R_{\rm GRB}$ is the GRB evolution rate, assumed to follow the star formation rate

$$R_{\rm GRB}(z) = \rho_0 \frac{R_{\rm SF}(z)}{R_{\rm SF}(z=0)},$$
$$R_{\rm SF}(z) = \frac{0.02 + 0.12z}{1 + (z/3.23)^{4.66}}. \tag{2}$$

In these equations, $R_{\rm SF}(z=0) = 0.02$ and $\rho_0 = 0.09 \pm 0.01\,{\rm Gpc}^{-3}\,{\rm yr}^{-1}$ (Howell & Coward 2013). We note that we do not need each value of the parameters, as we are only interested in selecting a given number of bursts. The volume element factor dV/dz is then given by

$$\frac{dV}{dz} = \frac{4\pi c}{H_0}\,\frac{d_L^2(z)}{(1+z)^2\,h(z)}\ , \tag{3}$$

where the $h(z)$ factor is the normalized Hubble parameter,

$$h(z) = H(z)/H_0 = [\Omega_M(1+z)^3 + \Omega_\Lambda]^{1/2}\ , \tag{4}$$

and the $d_L(z)$ is the luminosity distance evaluated using the fit formula of Pen (1999).

As for the luminosity distribution functions, we used those of Howell & Coward (2013) and Liang et al. (2007), and a customized version of the latter.

The first luminosity distribution function is assumed to be a power law with an exponential cutoff at low luminosity (Howell & Coward 2013)

$$\phi(L) = \phi_0 \left(\frac{L}{L_*}\right)^{-\alpha} \exp\left(\frac{L_*}{L}\right), \tag{5}$$

where $L_* = 2 \times 10^{52}$ erg s^{-1}, $\alpha = 3.8$ and we assume there is no luminosity evolution with redshift.

We used a null hypothesis that the whole population of GRBs at redshift $z < 1$ can be reproduced by this luminosity function. We bootstrap the redshift distribution function of 84 GRBs at $z < 1$ using a MC simulation. Note that the theoretical *Swift*-BAT detection sensitivity, $F_{\rm Lim} = 0.4\,{\rm ph\,s^{-1}\,cm^{-2}}$, was taken into account during the simulations. A K-S test was used to compare the theoretically expected to simulated distributions. This whole procedure was repeated 10^4 times to calibrate the K-S test distribution for our null hypothesis (see Figure 6, left). A calibrated Gaussian estimator was then obtained to test the real distribution K-S test (see Figure 6, right). We found that $D_n = 1.82$, which corresponds to a probability of 99% to be rejected. Thereby, we concluded that this luminosity function will unlikely reproduce our data.

We then tried the following broken power-law function of Liang et al. (2007):

$$\phi(L) = \phi_0 \left[\left(\frac{L}{L_b}\right)^{\alpha_1} + \left(\frac{L}{L_b}\right)^{\alpha_2}\right]^{-1}. \tag{6}$$

The fit parameters ($L_b = 1.72 \times 10^{51}$ erg s^{-1}, $\alpha_1 = 1.02$, $\alpha_2 = 2.51$) were taken from Deng et al. (2016). The luminosity limits are chosen to be 10^{49}–10^{54} erg s^{-1}. Using the procedure presented above, we find the null hypothesis value to be $D_n = 1.62$, which reflects a probability of 99.75% (see Figure 6). This null hypothesis was rejected at the 3σ level.

Last, we customized the luminosity function of Liang et al. (2007) by adding an exponential cutoff at 3×10^{48} erg s^{-1}. This was carried out as it increased the number of close events over distant ones. Its null hypothesis and probability were $D_n = 1.12$ and 91.57% (see Figure 6), respectively, which lies between the 3σ–2σ levels. Based on this customization as a means to fit our data as best as possible, we conclude that this luminosity function is an unlikely candidate for describing our sample.

A similar conclusion was reached by Liang et al. (2007), who showed that it was impossible to reproduce the observed volume density of low-redshift GRBs, as the local event rate would be dominated by low-luminosity GRBs. In this case, it is necessary to have two populations for low- and high-luminosity GRBs. By considering high and low-luminosity GRBs separately using the luminosity functions of Howell & Coward (2013) and Liang et al. (2007), our null hypotheses are rejected with probabilities of 23.09% or 37.24% (depending upon the selected luminosity function), and 99.999%, respectively. In other words, it is acceptable for high-luminosity events, while being strongly rejected for the population of low-luminosity events. This leads us to conclude that group III GRBs seem to form a different population than "classical" lGRBs.

4.3. Geometry and Environment of the Burst

Several authors (e.g., Yamazaki et al. 2003; Ramirez-Ruiz et al. 2005; Daigne & Mochkovitch 2007) have sought to explain some group III events via jet properties (aperture angle, viewing angle). For these authors, their group III events were either seen off-axis, or had a larger aperture angle of their jet.

The closure relations (Mészáros et al. 1998; Sari et al. 1998, 1999; Chevalier & Li 2000; Zhang & Mészáros 2008) allow investigations of the burst geometry, the fireball microphysics, its cooling state, and the surrounding medium. These are presented in Figure 7, which shows for our sample they are similar to the ones obtained from *BeppoSAX*, *XMM-Newton* or *Chandra* (De Pasquale et al. 2006; Gendre et al. 2006) for long bursts. We note, however, two peculiar events plus a third, less certain one.

1. GRB 120729A: the pre-jet break closure relations are rejected for this event, which is compatible only with the post-jet break closure relations. There is a break in the light curve at $t_b = 8.1$ ks, and the values of the temporal decay before this break are compatible with the pre-jet break closure relations (green points in Figure 7). Thus, we tentatively associate this temporal break with the jet break and deduce the positions of the specific frequencies and the value of p ($\nu_m < \nu_{\rm XRT} < \nu_c$, $p = 2.8 \pm 0.2$). There is also a hint of achromaticity, as this break is seen both in X-ray and in optical (D'Avanzo et al. 2012a; Maselli et al. 2012), supporting the interpretation of a jet effect.
2. GRB 161129A: this event is also not compatible with the pre-jet break closure relations, and its steep decay would perfectly fit a post-jet break light curve. However, a jet break could not be defined in the light curve. In the standard model, this implies an extremely closed jet (see Equation (7)).

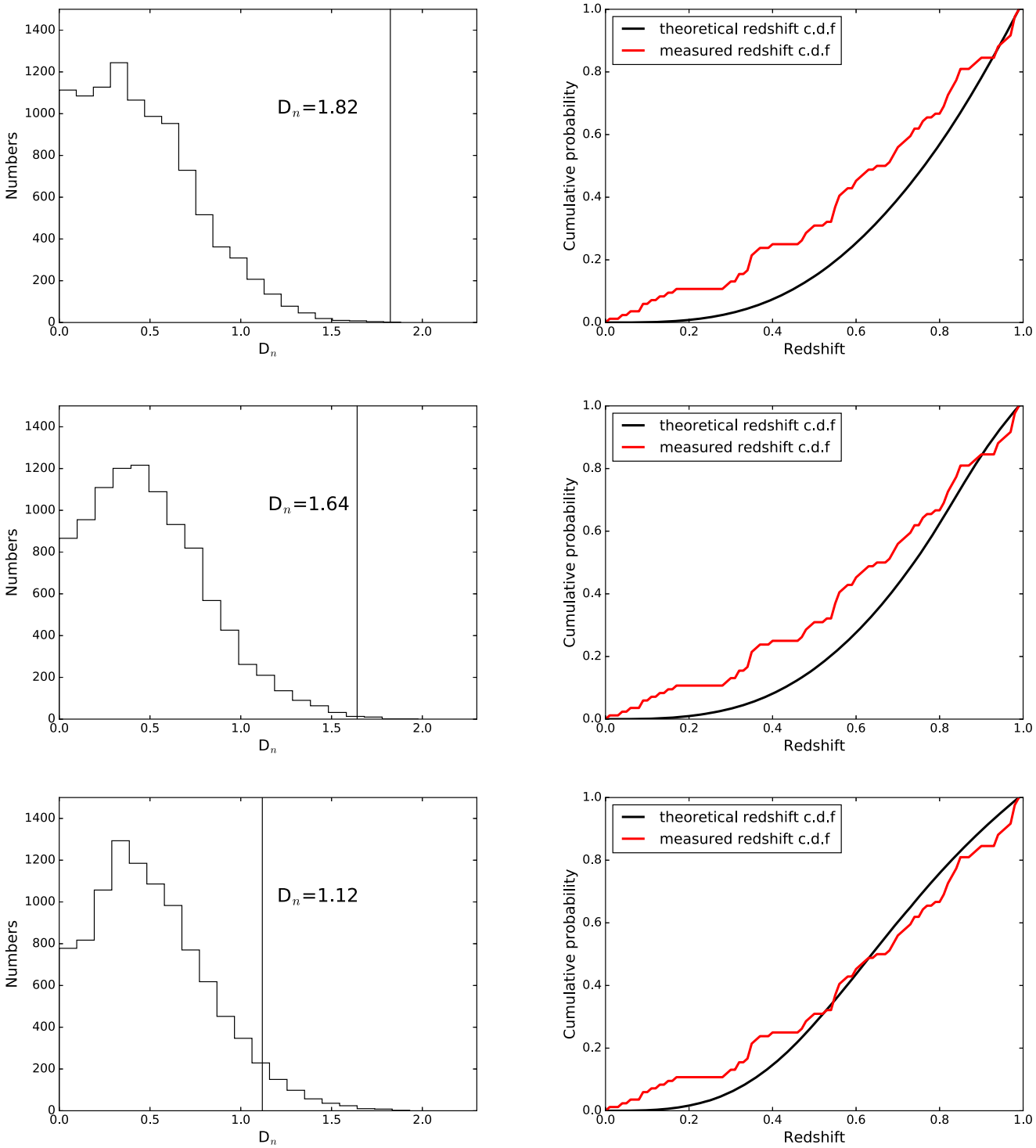

Figure 6. Left: the distribution of K-S values (D_n) from the MC simulation with 10,000 iterations for the sample of 84 GRBs. Right: the cumulative distribution functions of the theoretically expected redshift (black) and measured redshift values of 84 GRBs at redshift <1 (red). Each K-S value (D_n) is presented by a black line in left-hand panels by using (top) the LF from Howell & Coward (2013), (middle) the LF from Liang et al. (2007), and (bottom) the LF from Liang et al. (2007) plus exponential cutoffs.

3. GRB 060614: finally, this event would be compatible with another jet effect, with $p = 2.25 \pm 0.05$. However, the error bars are large enough to accommodate some non-jetted closure relations. We cannot conclude firmly on the jet hypothesis for this source based on the closure relations alone.

The opening angle is given by Levinson & Eichler (2005), who extended the work of Sari et al. (1999) to account for the radiation efficiency of the prompt phase,

$$\theta(t_b, E_{\rm iso}) = 0.161\left(\frac{t_{b,d}}{1+z}\right)^{3/8} n^{1/8}\left(\frac{\eta_\gamma}{E_{\rm iso,52}}\right)^{1/8}, \qquad (7)$$

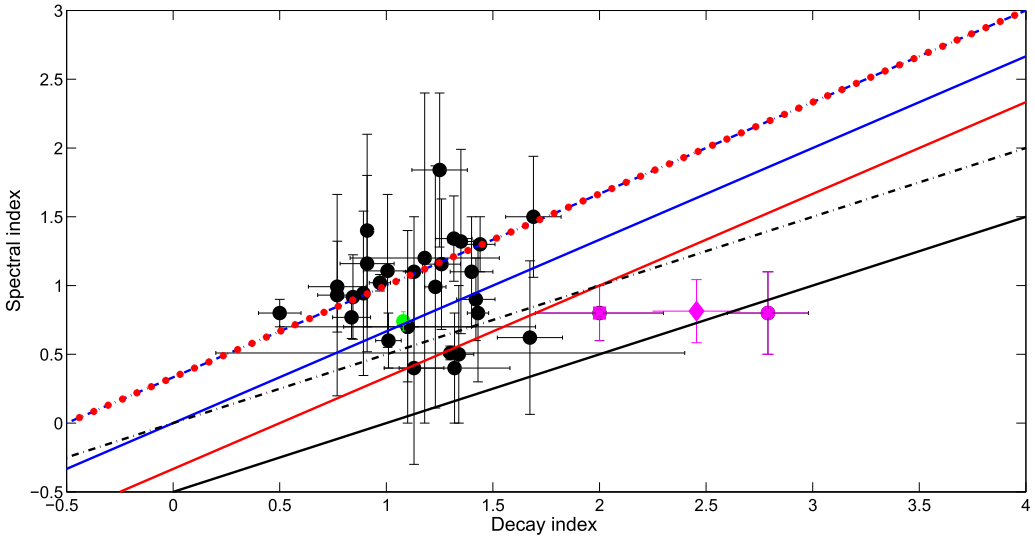

Figure 7. X-ray decay index vs. spectral index of the group III GRBs. The purple filled square, diamond, and circle represent GRB 060614, GRB 161129A, and GRB 120729A, respectively. The green dot represents GRB 120729A before the break at $t_b = 8.1$ ks. All closure relations, indicated by the lines, are computed for $p > 2$ in the slow cooling phase. Solid and dashed–dotted lines stand for $\nu_m < \nu < \nu_c$ and $\nu_c < \nu$ respectively. Blue, red, and black lines stand for ISM, wind medium, and jet effect, respectively.

where the standard values for the number density of the medium $n = 1\ \mathrm{cm}^{-3}$, the radiative efficiency $\eta_\gamma = 0.2$ and $E_{\mathrm{iso},52} = 2.3$ are used. For GRB 120729A, we obtained $\theta = 2\overset{\circ}{.}7$, which is coherent with the results of Cano et al. (2014), who used a different value for $E_{\mathrm{iso},52}$.

If we do not restrict ourselves to only X-ray results, a few other group III events also show jet properties, which we highlight as follows. GRB 011121 has a very clear jet break signature at 1.5 days (see, e.g., Zeh et al. 2006). A jet break is also likely for GRB 050525A at 0.3 days, as seen in optical data (Kann et al. 2010). Finally, a jet break is possible for GRB 081007 at 1.5 days, (see, e.g., Kann et al. 2016, and references therein). These values give a jet opening angle of only a few degrees in range. Thus, we conclude from these findings that in the presence of a jet aperture measurement, our results are similar to normal lGRBs (Ghisellini 2012, $\theta = 4\overset{\circ}{.}7 \pm 2\overset{\circ}{.}3$).

In regards to whether we are seeing the jet far off-axis, we emphasize, that the presence of jet breaks in our results implies near on-axis observations. However, such evidence does not rule out the presence of slightly off-axis observations for other event's data. Nonetheless, we find confidence in rejecting this hypothesis for our bursts where jet breaks were found.

For consistency, we also checked the burst environment. Most of the events in our sample can be explained by both a wind environment and a constant-density circumburst medium. Note that statistically more GRB afterglows provide evidence for a constant circumburst medium over that of the wind hypothesis (Schulze et al. 2011). Though, as many of these sources are associated with SNe (see Table 3), such would favor a wind environment. Given that Gendre et al. (2007) showed the termination shock can lie very close to the star, we cannot firmly conclude on the surrounding medium, nor its impacts to the various shocks generated by the burst in this work.

4.4. Microphysics of the Fireball

Several authors (e.g., Watson et al. 2004; Daigne & Mochkovitch 2007; Guetta & Della Valle 2007; Imerito et al. 2008) have proposed that several low-luminosity GRBs are mainly due to a difference in the microphysics of the fireball when compared with normal lGRBs. As all of these events are in our sample, we tested such a hypothesis by using the closure relations. Particularly because these relationships are useful for indicating the position of the cooling frequency and providing insight to the parameters of the fireball.

For most of the bursts in our sample, based on the presence of large uncertainties, we avoid making definitive conclusions about variations in fireball microphysics. However, an interesting aspect of this study was its evidence that the X-ray band was located *below* the cooling frequency for a few of them. This contradicts most late GRB afterglows, where the opposite is found (De Pasquale et al. 2006; Gendre et al. 2006). In that regard, and as this measurement is time dependent (Gendre et al. 2006), we insist that a comparison study with compatible data needs to be performed.

In the case of a constant-density circumburst medium, the formula of the cooling frequency is (Panaitescu & Kumar 2000)

$$\nu_c = 3.7 \times 10^{14} E_{53}^{-1/2} n^{-1} (Y+1)^{-2} \epsilon_{B,-2}^{-3/2} T_d^{-1/2}\ \mathrm{Hz}, \quad (8)$$

where E_{53} is the isotropic energy in units of 10^{53} erg, $\epsilon_{B,-2}$ is the fraction of internal energy of the magnetic field in units of 10^{-2}, n is the number density of the medium in the units of cm^{-3}, Y is the Compton parameter, and T_d is the time expressed in days after the burst. In the case of a wind medium, the cooling frequency reads

$$\nu_c = 3.5 \times 10^{14} E_{53}^{1/2} A_*^{-2} (Y+1)^{-2} \epsilon_{B,-2}^{-3/2} T_d^{1/2}\mathrm{Hz}, \quad (9)$$

where A_* is the number density in the wind.

Here, note that only for our bursts where the position of the cooling frequency can be deciphered, we were able to place possible constraints on the model. We started by assuming that the fireball expands in the constant-density circumburst medium. The XRT band covers 7.2×10^{16} Hz to 2.4×10^{18} Hz, but we assume that ν_c is above 3.7×10^{18} Hz (i.e., slightly above the X-ray band) for simplicity. When assuming a

Table 3
GRB-SN Associations

GRB Name	Redshift	SN Identification	SN Name	SN Type	Host Type	Group III GRB	L_{iso} of GRB[a] (10^{49}erg s^{-1})	References
GRB 980425	0.0085	Spectral	SN1998bw	BL-Ic	Dwarf spiral (SbcD)	Yes	0.033	(1)
GRB 011121	0.36	Bump	SN2001ke	⋯	N/A	Yes	387	(2), (3), (4), (5)
GRB 021211	1.01	Spectral	SN2002lt	∼Ic	N/A	No	802	(6), (7)
GRB 030329	0.168	Spectral	SN2003dh	BL-Ic	Dwarf starburst	No	77	(8), (9), (10), (11), (7)
GRB 031203	0.105	Spectral	SN2003lw	BL-Ic	Irr Wolf-Rayet	Yes	0.56	(12), (13), (14), (15)
GRB 050525A	0.606	Spectral	SN2005nc	∼Ic	N/A	Yes	417	(16), (17)
GRB 060218	0.0331	Spectral	SN2006aj	BL-Ib/c	Dwarf Irr	Yes	0.02	(18), (19), (20), (21), (22), (23)
GRB 081007	0.5295	Spectral	SN2008hw	Ic	N/A	Yes	30	(24), (25)
GRB 091127	0.49	Bump	SN2009nz	BL-Ic	N/A	No	301	(26), (25), (7)
GRB 100316D	0.059	Spectral	SN2010bh	BL-Ic	Spiral blue	Yes	0.056	(27), (28), (29), (30)
GRB 101219B	0.55	Spectral	SN2010ma	Ic	N/A	No	12.7	(31), (25), (7)
GRB 120422A	0.283	Spectral	SN2012bz	Ib/c	N/A	Yes	0.44	(32), (33)
GRB 120714B	0.3984	Spectral	SN2012eb	I	No identification	Yes	0.7	(34), (35)
GRB 130215A	0.597	Spectral	SN2013ez	Ic	N/A	No	75.3	(36), (7)
GRB 990712	0.4331	Bump	⋯	⋯	Reddened starburst	No	50.5	(37), (7)
GRB 020405	0.68986	Bump	⋯	⋯	Wolf-Rayet	No	422	(27), (7)
GRB 041006	0.716	Bump	⋯	⋯	N/A	No	286	(7)
GRB 090618	0.54	Bump	⋯	⋯	N/A	No	349	(7)
GRB 020903	0.2506	Spectral	⋯	BL-Ic	Wolf-Rayet	No	0.42	(38), (39), (40), (7)
GRB 111209A	0.67702	Spectral	2011kl	Ic SL[b]	∼Dwarf[c]	No	9.76	(41), (42), (43), (7)
GRB 111211A	0.478	Spectral	⋯	BL-Ic	N/A	No	∼73	(7), (44), (45)

Notes.
[a] The L_{iso} values are calculated from the E_{iso} values which are given in the Table 1 and the values for other GRBs were taken from Cano et al. (2017).
[b] SL is Super Luminous.
[c] Low-luminosity blue compact dwarf.
References. GRB-SN associations: (1) Galama et al. 1998; (2) Bloom et al. 2002; (3) Garnavich et al. 2003; (4) Greiner et al. 2003; (5) Küpcü Yoldas et al. 2007; (6) Della Valle et al. 2003; (7) Cano et al. 2017; (8) Hjorth et al. 2003; (9) Kawabata et al. 2003; (10) Stanek et al. 2003; (11) Gorosabel et al. 2005; (12) Cobb et al. 2004; (13) Gal-Yam et al. 2004; (14) Thomsen et al. 2004; (15) Malesani et al. 2004; (16) Della Valle et al. 2006; (17) Blustin et al. 2006; (18) Pian et al. 2006; (19) Cobb et al. 2006; (20) Campana et al. 2006; (21) Ferrero et al. 2006; (22) Mirabal et al. 2006; (23) Ferrero et al. 2006; (24) Jin et al. 2013; (25) Olivares et al. 2015 ; (26) Berger et al. 2011; (27) Cano et al. 2011; (28) Olivares et al. 2012; (29) Bufano et al. 2012; (30) Izzo et al. 2017; (31) Sparre et al. 2011; (32) Melandri et al. 2012; (33) Schulze et al. 2014; (34) Klose et al. 2012; (35) Cummings et al. 2012; (36) Cano et al. 2014; (37) Christensen et al. 2004; (38) Hammer et al. 2006; (39) Soderberg et al. 2005; (40) Han et al. 2010; (41) Levan et al. 2014; (42) Kann et al. 2016; (43) Greiner et al. 2015; (44) de Ugarte Postigo et al. 2012; (45) Fan et al. 2013.

standard density $n = 1\ \mathrm{cm}^{-3}$, the Compton parameter $Y \ll 1$ and considering the observation time of 1 day, Equation (8) can be simplified to

$$10^{-4} E_{53}^{-1/2} \epsilon_{B,-2}^{-3/2} < 1. \quad (10)$$

Taking the lowest E_{53} measured (to have the most stringent constraint), i.e., 10^{-5} (value of E_{53} for GRB 980425), we obtain $\epsilon_{B,-2} > 0.1$, which is not really constraining, as typical values of $\epsilon_{B,-2}$ should be of the order of one for lGRBs. The situation is similar when assuming a wind medium, where Equation (9) implies

$$10^{-4} E_{53}^{1/2} \epsilon_{B,-2}^{-3/2} < 1, \quad (11)$$

when assuming a standard density. The difference between Equations (10) and (11) is the power of E_{53}. Thus, using the same method than before, but with the largest value of E_{53}, we obtain $\epsilon_{B,-2} > 0.0012$ from Equation (11).

It is clear, from the previous constraints, that even with an unusually low magnetic energy in the fireball it could not explain the position of the cooling frequency below the XRT band, independent of the medium surrounding the burst. We, thus, conclude that for both burst medium environments, the uncommon position of the cooling frequency for group III GRBs, compared to normal lGRBs, may be due to a small total energy, over the introduction of significant magnetic energy into the fireball.

4.5. Prompt Properties

In Figure 8, we clearly observe that the few possible outliers of the Amati relation are members of our group III GRB sample. Several explanations have been proposed previously for these events (see Amati 2006; Amati et al. 2007, and reference therein for details): GRB 060505 could be a short GRB (as its location in the $E_{p,i}$–E_{iso} plane hints to); the $E_{p,i}$ value of GRB 061021 refers to the first hard pulse, while a soft tail is present (so the true $E_{p,i}$ is possibly lower); GRB 031203 may be much softer than measured by *INTEGRAL*/ISGRI, notions supported by its *XMM-Newton* dust echo measurement (Sazonov et al. 2004; Watson et al. 2004, 2006).

The last argument of that list is interesting. We can indeed see that our outliers are all located in the left part of the $E_{p,i}$–E_{iso} plane. In this part of the diagram, the usual gamma-ray instruments are not well suited to measure the prompt properties. For instance, the BAT measurements of GRB 060218 (Sakamoto et al. 2006) would have made this event more similar to GRB 980425, i.e., a clear outlier. It is the simultaneous observations by BAT and XRT that makes it

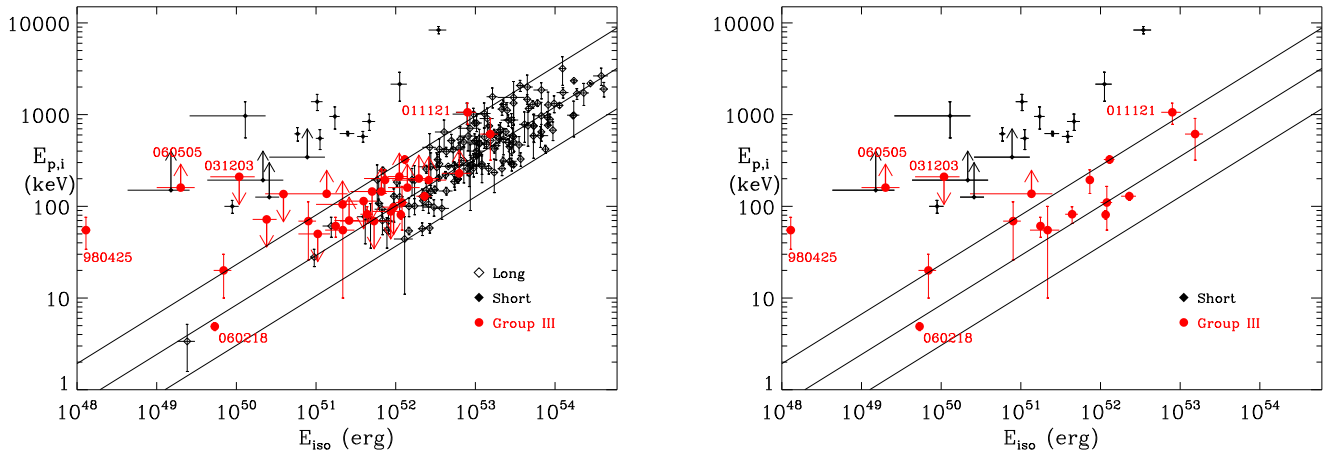

Figure 8. Location in the $E_{p,i}$–$E_{\rm iso}$ plane of the group III GRBs sample. Left: comparison of both short and long GRBs. Right: compared with short events, with firm measurements and non-compatible lower limits on $E_{p,i}$ only.

compatible with the Amati relation. One may imagine that this conclusion may hold for all outliers, and that all group III events are compatible with the Amati relation once corrected for observational biases. We note, however, that the prompt phase of a GRB usually shows a hard-to-soft spectral variation (e.g., Mészáros 2006), and that the prompt emission of GRB 060218 lasted significantly longer than other bursts. Thereby, it is not clear whether a measurement consistent with those performed at the *BeppoSAX* epoch (i.e., time averaged over the complete prompt emission) would lead to a similar conclusion.

Another hypothesis could be that the group III GRBs form a different population of bursts that result in another track in the Amati Relation. A flatter Amati relation has been foreseen as early as 2003 (Yamazaki et al. 2003), witnessed in off-axis GRBs. It is pointed out that a similar off-axis explanation holds in the case of the cannonball model (Dado & Dar 2005). If observed off-axis, the group III events are expected to be less luminous than normal lGRBs *even during the afterglow* (see e.g., D'Alessio et al. 2006). However, a balance of such arguments with the fact that group III events are detected is necessary. Particularly, as an off-axis observed burst's luminosity would decreases rapidly, at a decay rate related to the off-axis angle. The simple fact that these events are detected means that they are not at very large off-axis angles. Therefore, our study suggests they should be considered slightly off-axis, which, we emphasize, aligns with the finds of various groups (e.g., Salafia et al. 2016).

4.6. Link between Group III Events and Low-luminosity GRBs

In the past, several GRBs with a very faint prompt emission have been observed: GRB 980425 (e.g., Galama et al. 1998; Kulkarni et al. 1998), GRB 031203 (e.g., Malesani et al. 2004; Soderberg et al. 2004; Watson et al. 2004), GRB 060218 (e.g., Campana et al. 2006; Mazzali et al. 2006; Pian et al. 2006; Soderberg et al. 2006; Virgili et al. 2009) and GRB 100316D (e.g., Fan et al. 2011; Starling et al. 2011). These events are called low-luminosity GRBs and are all group III events.

Several theoretical works have sought to explain these events within the framework of the standard model (e.g., Daigne & Mochkovitch 2007; Barniol Duran et al. 2015). Interestingly, in most cases these works pointed out that such events should be understood as a different class of lGRBs, which agrees with our findings. Although an issue must be considered with these theoretical works, as their methods become more questionable when a single event's properties are extrapolated as a fit to a whole class of events. This clearly appears when one compares the properties of GRB 060218 with GRB 980425, which are very different, and claims that one is representative of the other.

To date, no previous study has used a large sample of *Swift* events as a means to statistically study the global properties of low-luminosity GRBs. If we assume that all group III GRBs are low-luminosity GRBs, such has been accomplished by this work. We recognize that there is no a priori explanation why the group III GRBs would have a low $E_{\rm iso}$ (and a low prompt luminosity). However, it is known that the prompt and afterglow luminosities are linked together (De Pasquale et al. 2006; Gehrels et al. 2008; Evans et al. 2009; Kann et al. 2010). In that regard, if a similar linkage of group III and low-luminosity GRBs is assumed, straightforwardly then the mean properties of GRBs with a low-luminosity afterglow derived in this paper might apply to low-luminosity GRBs.

5. Conclusions

In this paper we have studied a large sample of lGRB afterglow light curves. From this sample, we constructed a subsample of events based on their faint afterglow luminosity after the plateau phase. This subsample was called *group III GRBs*, and we showed that it was statistically significant. The hypothesis that these events represented the tail of the long normal GRBs' luminosity function was also tested and rejected.

We have derived the main properties of our group III GRB sample. On average, we found, our group III GRBs were closer than normal lGRBs, but that their A_V and $N_{\rm H}$ values were similar to these burst types. Most group III GRBs were identified as being consistent with the closure relations expected for the fireball model, and the few outliers to such, were reported to be accounted for by an early jet break. We have provided evidence that the group III events were also intrinsically fainter during their prompt phase, reinforcing the evidence for a different population. Actually, some events may not follow the $E_{p,i}$–$E_{\rm iso}$ relation holding for classical long GRBs.

Various claims on group III GRB properties have been reported for some peculiar members of the sample by other authors and then extended to the whole population of

underluminous events (or events with an underluminous afterglow). Based on the statistical significance of our sample, we were able to test these hypotheses using rigorous statistical methods. We have shown that to explain all these properties, one can invoke either geometrical arguments for the bursts, or different kinds of progenitors. In the former hypothesis, the bursts would be seen slightly off-axis to explain the low-energy budget observed in these events. In the latter, one could imagine that the progenitor provides less matter for the accretion, thus diminishing the energetic budget at start.

We thank Cristiano Guidorzi, at University of Ferrara, for providing help during the analysis of the BAT spectra. We are grateful for the comments and suggestions by the anonymous referee, which helped to improve the manuscript. This paper is under the auspices of the FIGARONet collaborative network, supported by the Agence Nationale de la Recherche, program ANR-14-CE33. We used the data supplied by the UK *Swift* Science Data Center at the University of Leicester. This work has been part of the H.D. PhD. thesis supported by the Erasmus Mundus Joint Doctorate Program by grant Number 2011-1640 from the EACEA of the European Commission. H.D. acknowledges financial support from Bilim Akademisi, The Science Academy, Turkey under the TÜBITAK-BAGEP program 1059B191500067. B.G. and N.B.O. acknowledge financial support of the NASA through the NASA Award NNX13AD28A and the NASA Award NNX15AP95A.

Facility: Swift.

Appendix
Sample Selection Method

To construct our sample, we used the XRT light curves retrieved from the online *Swift* repository[10] (Evans et al. 2009). The comparison of flux light curves needs a careful estimation of the spectral index and the count-to-flux conversion factor. We cannot use the data downloaded from the online repository directly because the estimation of these two parameters is done using standard models that do not correspond to our needs. We have to estimate the spectral index independently and the count-to-flux conversion factor. For this purpose, we also downloaded the raw data from the archives. We applied to all data the same calibration to avoid any instrumental effects (we used the version of caldb dated 2013 May, and the HEASOFT package version 6.12).[11]

Each spectrum was fitted with a power-law model absorbed twice: once by the host galaxy and once by the Milky Way Galaxy. The $N_{\rm H}$ value of the Galaxy was set to the value given by the Leiden/Argentine/Bonn (LAB) Survey of Galactic H I (Kalberla et al. 2005), while the one for the host was let free to vary at the host redshift. We derived from this model a count-to-flux conversion factor to translate the count light curves of the repository into a 2.0–10.0 keV band flux light curve (we chose this band to neglect the absorption while comparing the data).

Each light curve is then filtered following the method of Gendre et al. (2008). We removed from the light curves all emissions present before the end of the plateau phase and all flaring emissions. These net light curves were finally corrected by taking into account the cosmological effects through the K-correction. We worked on a "flux" light curve, rescaling all light curves to a common distance of $z = 1$. As stated in Gendre & Boër (2005), this allows for a smaller uncertainty in the final light curves. Consider for instance the following equation,

$$K \propto (1 + z)^{\beta}. \tag{12}$$

One can see that the K-correction is very sensitive to the spectral index. With a redshift of 4 and a precision of 1.0 ± 0.3 for β, the uncertainty on K is 5 ± 3, i.e., 60%. Rescaling to $z = 1$ leads to 2.5 ± 0.7, i.e., an uncertainty of 28%: this method reduces the scattering induced by the uncertainties on the measurements, allowing for a more precise selection of the sample.

[10] http://www.swift.ac.uk/xrt_curves
[11] http://heasarc.gsfc.nasa.gov/heasoft/

ORCID iDs

H. Dereli https://orcid.org/0000-0002-8852-7530
M. Boër https://orcid.org/0000-0001-9157-4349
B. Gendre https://orcid.org/0000-0002-9077-2025
L. Amati https://orcid.org/0000-0001-5355-7388
N. B. Orange https://orcid.org/0000-0001-6866-1436

References

Amati, L. 2006, MNRAS, 372, 233
Amati, L., Della Valle, M., Frontera, F., et al. 2007, A&A, 463, 913
Amati, L., Frontera, F., & Guidorzi, C. 2009, A&A, 508, 173
Amati, L., Frontera, F., Tavani, M., et al. 2002, A&A, 390, 81
Barniol Duran, R., Nakar, E., Piran, T., & Sari, R. 2015, MNRAS, 448, 417
Barthelmy, S. D., Cannizzo, J. K., Gehrels, N., et al. 2005, ApJL, 635, L133
Berger, E., Chornock, R., Holmes, T. R., et al. 2011, ApJ, 743, 204
Bhat, P. N. 2011, GCN Circ., 11543
Bissaldi, E., McBreen, S., & Connaughton, V. 2008, GCN Circ., 8369
Bloom, J. S., Kulkarni, S. R., Price, P. A., et al. 2002, ApJL, 572, L45
Blustin, A. J., Band, D., Barthelmy, S., et al. 2006, ApJ, 637, 901
Boër, M., & Gendre, B. 2000, A&A, 361, L21
Bufano, F., Pian, E., Sollerman, J., et al. 2012, ApJ, 753, 67
Cabrera, G. F., Casassus, S., & Hitschfeld, N. 2008, ApJ, 672, 1272
Campana, S., Mangano, V., Blustin, A. J., et al. 2006, Natur, 442, 1008
Cano, Z., Bersier, D., Guidorzi, C., et al. 2011, ApJ, 740, 41
Cano, Z., de Ugarte Postigo, A., Pozanenko, A., et al. 2014, A&A, 568, A19
Cano, Z., Wang, S. Q., Dai, Z. G., & Wu, X. F. 2017, AdAst, 2017, 8929054
Chevalier, R. A., & Li, Z. Y. 2000, ApJ, 536, 195
Christensen, L., Hjorth, J., Gorosabel, J., et al. 2004, A&A, 413, 121
Cobb, B. E., Bailyn, C. D., van Dokkum, P. G., et al. 2004, ApJL, 608, L93
Cobb, B. E., Bailyn, C. D., van Dokkum, P. G., & Natarajan, P. 2006, ApJL, 645, L113
Costa, E., Frontera, F., Heise, J., et al. 1997, Natur, 387, 783
Covino, S., Melandri, A., Salvaterra, R., et al. 2013, MNRAS, 432, 1231
Coward, D. M. 2005, MNRAS, 360, L77
Coward, D. M., Howell, E. J., Branchesi, M., et al. 2013, MNRAS, 432, 2141
Cummings, J. R., Barthelmy, S. D., Baumgartner, W. H., et al. 2012, GCN Circ., 13481
Dado, S., & Dar, A. 2005, ApJL, 627, L109
Daigne, F., & Mochkovitch, R. 2007, A&A, 465, 1
D'Alessio, V., Piro, L., & Rossi, E. M. 2006, A&A, 460, 653
D'Avanzo, P., Melandri, A., Steele, I., Mundell, C. G., & Palazzi, E. 2012a, GCN, 13551
D'Avanzo, P., Salvaterra, R., Sbarufatti, B., et al. 2012b, MNRAS, 425, 506
De Pasquale, M., Piro, L., Gendre, B., et al. 2006, A&A, 455, 813
de Ugarte Postigo, A., Thoene, C. C., & Gorosabel, J. 2012, GCN, 12802
Della Valle, M., Malesani, D., Benetti, S., et al. 2003, A&A, 406, L33
Della Valle, M., Malesani, D., Bloom, J. S., et al. 2006, ApJL, 642, L103
Deng, C. M., Wang, X. G., & Guo, B. B. 2016, ApJ, 820, 66
Dezalay, J. P., Barat, C., Talon, R., et al. 1992, in AIP Conf. Proc. 265, Proc. Gamma-ray Bursts Workshop, ed. W. S. Paciesas & G. J. Fishman (Melville, NY: AIP), 304
Eichler, D., Livio, M., Piran, T., & Schramm, D. N. 1989, Natur, 340, 126
Evans, P. A., Beardmore, A. P., Page, K. L., et al. 2009, MNRAS, 397, 1177
Fan, Y.-Z., Tam, P. H. T., Zhang, F.-W., et al. 2013, ApJ, 776, 95
Fan, Y. Z., Zhang, B. B., Xu, D., Liang, E. W., & Zhang, B. 2011, ApJ, 726, 32

Ferrero, P., Kann, D. A., Zeh, A., et al. 2006, A&A, 457, 857
Frail, D. A., Kulkarni, S. R., Nicastro, L., et al. 1997, Natur, 389, 261
Galama, T. J., Vreeswijk, P. M., van Paradijs, J., et al. 1998, Natur, 395, 670
Gal-Yam, A., Moon, D.-S., Fox, D. B., et al. 2004, ApJL, 609, L59
Garnavich, P. M., Stanek, K. Z., Wyrzykowski, L., et al. 2003, ApJ, 582, 924
Gehrels, N., Barthelmy, S. D., Burrows, D. N., et al. 2008, ApJ, 689, 1161
Gehrels, N., Chincarini, G., Giommi, P., et al. 2004, ApJ, 611, 1005
Gendre, B., & Boër, M. 2005, A&A, 430, 465
Gendre, B., Corsi, A, Piro, L., et al. 2006, A&A, 455, 803
Gendre, B., Galli, A., & Boër, M. 2008, ApJ, 683, 620
Gendre, B., Galli, A., Corsi, A, et al. 2007, A&A, 462, 565
Ghisellini, G. 2012, arXiv:1211.2062
Ghisellini, G., Nardini, M., Ghirlanda, G., & Celotti, A. 2009, MNRAS, 393, 253
Gorosabel, J., Pérez-Ramírez, D., Sollerman, J., et al. 2005, A&A, 444, 711
Greiner, J., Klose, S., Salvato, M., et al. 2003, ApJ, 599, 1223
Greiner, J., Krühler, T., Klose, S., et al. 2010, in AIP Conf. Ser. 1279, Deciphering the Ancient Universe with Gamma-ray Bursts, ed. N. Kawai & S. Nagataki (Melville, NY: AIP), 144
Greiner, J., Mazzali, P. A., Kann, D. A., et al. 2015, Natur, 523, 189
Guetta, D., & Della Valle, M. 2007, ApJL, 657, L73
Hammer, F., Flores, H., Schaerer, D., et al. 2006, A&A, 454, 103
Han, X. H., Hammer, F., Liang, Y. C., et al. 2010, A&A, 514, A24
Hjorth, J., Sollerman, J., Møller, P., et al. 2003, Natur, 423, 847
Holland, S. T., Sbarufatti, B., Shen, R., et al. 2010, ApJ, 717, 223
Howell, E. J., & Coward, D. M. 2013, MNRAS, 428, 167
Imerito, A., Coward, D., Burman, R., & Blair, D. 2008, MNRAS, 391, 405
Izzo, L., Thöne, C. C., Schulze, S., et al. 2017, MNRAS, 472, 4480
Jakobsson, P., Hjorth, J., Fynbo, J. P. U., et al. 2004, ApJL, 617, L21
Jakobsson, P., Levan, A., Fynbo, J. P. U., et al. 2006, A&A, 447, 897
Jin, Z. P., Covino, S., Della Valle, M., et al. 2013, ApJ, 774, 114
Kalberla, P. M. W., Burton, W. B., Hartmann, Dap., et al. 2005, A&A, 440, 775
Kann, D. A., Klose, S., Zeh, A., et al. 2006, ApJ, 641, 993
Kann, D. A., Klose, S., Zhang, B., et al. 2010, ApJ, 720, 1513
Kann, D. A., Klose, S., Zhang, B., et al. 2011, ApJ, 734, 96
Kann, D. A., Schady, P., Olivares, E. F., et al. 2016, arXiv:1606.06791
Kawabata, K. S., Deng, J., Wang, L., et al. 2003, ApJL, 593, L19
Klose, S., Greiner, J., Fynbo, J., et al. 2012, CBET, 3200
Kouveliotou, C., Meegan, C. A., Fishman, G. J., & Bhat, N. P. 1993, ApJL, 413, L101
Krühler, T., Kuncarayakti, H., Schady, P., et al. 2017, A&A, 602, A85
Kulkarni, S. R., Frail, D. A., Wieringa, M. H., et al. 1998, Natur, 395, 663
Kumar, P., & Zhang, B. 2015, PhR, 561, 109 1
Küpcü Yoldaş, A., Salvato, M., Greiner, J., et al. 2007, A&A, 463, 893
Levan, A. J., Tanvir, N. R., & Starling, R. L. C. 2014, ApJ, 781, 13
Levinson, A., & Eichler, D. 2005, ApJL, 629, L13
Liang, E., & Zhang, B. 2006, ApJL, 638, L67
Liang, E., Zhang, B., Virgili, F., & Dai, G. 2007, ApJ, 662, 1111
Malesani, D., Tagliaferri, G., Chincarini, G., et al. 2004, ApJL, 609, L5
Mannucci, F., Salvaterra, R., & Campisi, M. A. 2011, MNRAS, 414, 1263
Marshall, F. E., Antonelli, L. A., Burrows, D. N., et al. 2011, ApJ, 727, 132
Maselli, A., Burrows, D. N., Kennea, J. A., et al. 2012, GCN Circ., 13541
Maselli, A., Melandri, A., Nava, L., et al. 2014, Sci, 343, 48
Mazets, E. P., Golenetskii, S. V., Ilinskii, V. N., et al. 1981, Ap&SS, 80, 3
Mazzali, P. A., Deng, J., Nomoto, K., et al. 2006, Natur, 442, 1018
Melandri, A., Guidorzi, C., Kobayashi, S., et al. 2009, MNRAS, 395, 1941
Melandri, A., Pian, E., Ferrero, P., et al. 2012, A&A, 547, A82
Mészáros, P. 2006, RPPh, 69, 2259
Mészáros, P., & Rees, M. J. 1997, ApJ, 476, 232
Mészáros, P., Rees, M. J., & Wijers, R. A. M. I. 1998, ApJ, 499, 301
Michalowski, M. J., Kamble, A., Hjorth, J., et al. 2012, ApJ, 755, 85
Mirabal, N., Halpern, J. P., An, D., Thorstensen, J. R., & Terndrup, D. M. 2006, ApJL, 643, L99
Morrison, R., & McCammon, D. 1983, ApJ, 270, 119
Nardini, M., Ghisellini, G., Ghirlanda, G., et al. 2006, A&A, 451, 821
Nousek, J. A., Kouveliotou, C., Grube, D., et al. 2006, ApJ, 642, 389
Olivares, E. F., Greiner, J., Schady, P., et al. 2012, A&A, 539, A76
Olivares, E. F., Greiner, J., Schady, P., et al. 2015, A&A, 577, A44
Panaitescu, A., & Kumar, P. 2000, ApJ, 543, 66
Panaitescu, A., Mészáros, P., & Rees, M. J. 1998, ApJ, 503, 314
Pe'er, A. 2015, AdAst, 2015, 907321
Pen, U. L. 1999, ApJS, 120, 49
Perley, D. A., Cenko, S. B., Bloom, J. S., et al. 2009, AJ, 138, 1690
Pian, E., Amati, L., Antonelli, L. A., et al. 1999, A&AS, 138, 463
Pian, E., Mazzali, P. A., Masetti, N., et al. 2006, Natur, 442, 1011
Ramirez-Ruiz, E., Granot, J., Kouveliotou, C., et al. 2005, ApJL, 625, L91
Rees, M. J., & Mészáros, P. 1992, MNRAS, 258, 41
Reichart, D. E., & Price, P. A. 2002, ApJ, 565, 174
Sakamoto, T., Barbier, L., Barthelmy, S., et al. 2006, GCN Circ., 4822
Sakamoto, T., Barthelmy, S. D., Baumgartner, W. H., et al. 2011, ApJS, 195, 2
Salafia, O. S., Ghisellini, G., Pescalli, A., Ghirlanda, G., & Nappo, F. 2016, MNRAS, 461, 3607
Sari, R. 1999, ApJL, 524, L43
Sari, R., Piran, T., & Halpern, J. P. 1999, ApJL, 519, L17
Sari, R., Piran, T., & Narayan, R. 1998, ApJL, 497, L17
Sazonov, S. Y., Lutovinov, A. A., & Sunyaev, R. A. 2004, Natur, 430, 646
Schady, P., Dwelly, T., Page, M. J., et al. 2012, A&A, 537, A15
Schlafly, E. F., & Finkbeiner, D. P. 2011, ApJ, 737, 103
Schulze, S., Klose, S., Björnsson, G., et al. 2011, A&A, 526, A23
Schulze, S., Malesani, D., Cucchiara, A., et al. 2014, A&A, 566, A102
Soderberg, A., Berger, E., & Schmidt, B. 2006, IAUC, 8674, 2
Soderberg, A. M., Kulkarni, S. R., Berger, E., et al. 2004, Natur, 430, 648
Soderberg, A. M., Kulkarni, S. R., Fox, D. B., et al. 2005, A&A, 627, 777
Sparre, M., Sollerman, J., Fynbo, J. P. U., et al. 2011, ApJL, 735, L24
Stanek, K. Z., Matheson, T., Garnavich, P. M., et al. 2003, ApJL, 591, L17
Starling, R. L. C., Wiersema, K., Levan, A. J., et al. 2011, MNRAS, 411, 2792
Starling, R. L. C., Willingale, R., Tanvir, N. R., et al. 2013, MNRAS, 431, 3159
Tagliaferri, G., Goad, M., Chincarini, G., et al. 2005, Natur, 436, 985
Thomsen, B., Hjorth, J., Watson, D., et al. 2004, A&A, 419, L21
Thöne, C. C., de Ugarte Postigo, A., Fryer, C. L., et al. 2011, Natur, 480, 72
Thöne, C. C., Fynbo, J. P. U., Östlin, G., et al. 2008, ApJ, 676, 1151
Ulanov, M. V., Golenetskii, S. V., Frederiks, D. D., et al. 2005, NCimC, 28, 351
Van Paradijs, J., Groot, P. J., Galama, T., et al. 1997, Natur, 386, 686
Virgili, F. J., Liang, E. W., & Zhang, B. 2009, MNRAS, 392, 91
Watson, D., Hjorth, J., Levan, A., et al. 2004, ApJL, 605, L101
Watson, D., Vaughan, S. A., Willingale, R., et al. 2006, ApJ, 636, 967
Willingale, R., O'Brien, P. T., Osborne, J. P., et al. 2007, ApJ, 662, 1093
Woosley, S. E. 1993, ApJ, 405, 273
Yamazaki, R., Yonetoku, D., & Nakamura, T. 2003, ApJL, 594, L79
Zafar, T., Watson, D., Fynbo, J. P. U., et al. 2011, A&A, 532, A143
Zeh, A., Klose, S., & Kann, D. A. ApJ, 637, 889
Zhang, B., Fan, Y. Z., Dyks, J., et al. 2006, ApJ, 642, 354
Zhang, B., & Mészáros, P. 2008, IJMP, 19, 2385